

Compressive behaviour and micromechanical modelling of steel-reinforced resin under monotonic and cyclic loading

Christoforidou, Angeliki; Baskar, Abishek; Kane, Entela; Pavlovic, Marko

10.1016/j.compscitech.2025.111387

Publication date

Document Version Final published version

Published in

Composites Science and Technology

Citation (APA)

Christofòridou, A., Baskar, A., Kane, E., & Pavlovic, M. (2025). Compressive behaviour and micromechanical modelling of steel-reinforced resin under monotonic and cyclic loading. *Composites Science and Technology*, *272*, Article 111387. https://doi.org/10.1016/j.compscitech.2025.111387

Important note

To cite this publication, please use the final published version (if applicable). Please check the document version above.

Copyright

Other than for strictly personal use, it is not permitted to download, forward or distribute the text or part of it, without the consent of the author(s) and/or copyright holder(s), unless the work is under an open content license such as Creative Commons.

Please contact us and provide details if you believe this document breaches copyrights. We will remove access to the work immediately and investigate your claim.

ELSEVIER

Contents lists available at ScienceDirect

Composites Science and Technology

journal homepage: www.elsevier.com/locate/compscitech



Compressive behaviour and micromechanical modelling of steel-reinforced resin under monotonic and cyclic loading

Angeliki Christoforidou ^a, Abishek Baskar ^a, Entela Kane ^b, Marko Pavlovic ^{a,*}

ARTICLE INFO

Keywords:
Steel reinforced resin
Compression
Monotonic
Confinement
Fatigue
Triaxial test
Micro-mechanics

ABSTRACT

Steel-Reinforced Resin (SRR) is a particulate material originally developed as an injectant for anchoring applications. More recently, it has been proposed as a filler material for cavities embedding mechanical connectors in FRP-steel hybrid bridges. In this context, the compressive behaviour of SRR becomes critical due to the multi-axial stress states and fatigue demands at a joint scale. This paper presents a comprehensive experimental and numerical investigation of SRR under monotonic, incremental cyclic, and fatigue compressive loading in unconfined conditions. A custom triaxial setup is also used to evaluate pressure sensitivity and strength enhancement due to confinement under monotonic loading. In parallel, micromechanical finite element models are developed to simulate the interactions between the resin matrix and the steel balls at the microscale, incorporating interface damage, friction, and cohesive failure. The models reproduce the observed nonlinear behaviour and reveal distinct Poisson's ratio responses in tension and compression, offering deeper insight into the mechanisms governing stiffness degradation, strain softening, and plateau behaviour.

1. Introduction

Steel-Reinforced Resin (SRR) is a particulate composite material composed of densely packed steel particles embedded in a polymer matrix. Originally developed as an injectant for anchoring applications, as shown Fig. 1a [1], SRR has more recently been proposed as a filler material in cavities embedding mechanical connectors for FRP-steel hybrid bridges, as illustrated in Fig. 1b [2–6]. To provide a more tangible understanding of the SRR connector system, Fig. 2 presents an actual cut section of an SRR-filled connector embedded in an FRP sandwich panel. The steel particles and resin components are highlighted to illustrate the material's particulate structure. In these applications, SRR is subjected to multiaxial stress states, cyclic compressive loads, and confinement by surrounding structural elements, making its compressive and fatigue behaviour critical for long-term joint performance.

Due to its granular nature and high steel content, SRR is expected to exhibit pressure-sensitive mechanical behaviour. This aligns with the behaviour of other granular composites, where lateral confinement is known to enhance compressive strength and deformation capacity by In granular composite materials, it is well established that lateral confinement increases both compressive strength and deformation capacity [8]. Furthermore, shear strength is enhanced under confinement, as the tighter contact between particles reduces their ability to rearrange or slide, thereby increasing overall stability and resistance to shear forces. Comparable effects of hydrostatic confinement have been observed in ceramic matrix composites, where failure mechanisms evolve from microcracking to shear banding as pressure increases [9]. Recent studies on epoxy polymer concrete, another particulate resin-based composite, have shown that confinement significantly enhances its strength and deformation capacity, shifting its behaviour from strain softening to pseudo-ductility under higher confining pressures [10]. These findings reinforce the importance of investigating the

E-mail address: m.pavlovic@tudelft.nl (M. Pavlovic).

^a Steel and Composite Structures, Department of Engineering Structures, Faculty of Civil Engineering and Geosciences, Delft University of Technology, Stevinweg 1, Delft, 2628 CN, South Holland, the Netherlands

b Rock Deformation Laboratory, Department of Geosciences and Engineering, Faculty of Civil Engineering and Geosciences, Delft University of Technology, Stevinweg 1, Delft, 2628 CN, South Holland, the Netherlands

restricting particle rearrangement and increasing internal friction. Triaxial test methods are widely adopted to evaluate the shear resistance and strength of granular composites under various conditions of axial loading and confining pressure. Initially developed for soil research, triaxial testing gained popularity for asphalt mixtures in the 1950s. In 1969, the exploration of biaxial and triaxial stress states was extended to normal-strength concrete [7].

^{*} Corresponding author.

confined compressive response of resin-based granular composites such as SRR.

Previous studies on SRR have hinted at this pressure sensitivity. Nijgh, who originally developed the material [1], applied the Drucker-Prager model to capture its behaviour under confined and unconfined loading conditions [11]. The effect of confinement to the SRR material has not yet been studied using a triaxial test setup. Instead, lateral confinement was passively applied by both Nijgh and Pedrosa using a 4 mm thick steel tube, while the load was introduced to the SRR cylindrical specimen through a solid steel pin [11,12]. Static tests conducted by Nijgh and quasi-static cyclic tests by Pedrosa both demonstrated that full confinement increases the stiffness of SRR. Pedrosa particularly noted that this effect becomes more pronounced after a larger number of cycles, once the material undergoes settlement and densification [12]. While both static and cyclic tests confirmed that confinement improves SRR stiffness, especially after material settlement due to cycling, the steel tube itself yielded before the SRR reached its compressive limit, making the setup unsuitable for strength characterization.

When SRR is used as an injection material for injection bolts, it is surrounded by metallic components, where the confining pressure is assumed to be very high. On the contrary, in FRP applications, the injected material is surrounded by the composite bottom facing and the foam core of the sandwich panel web. The contribution of the foam core to load transfer is considered negligible, while the composite bottom facing offers less rigid boundary conditions compared to confinement

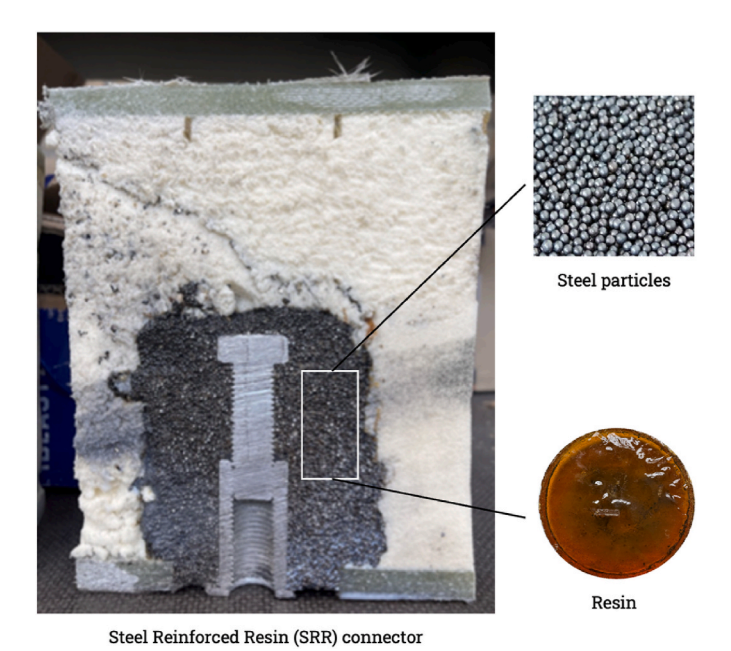
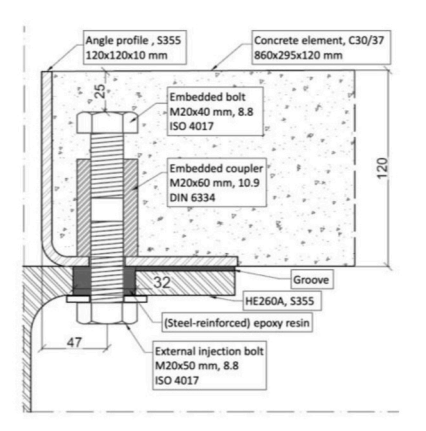
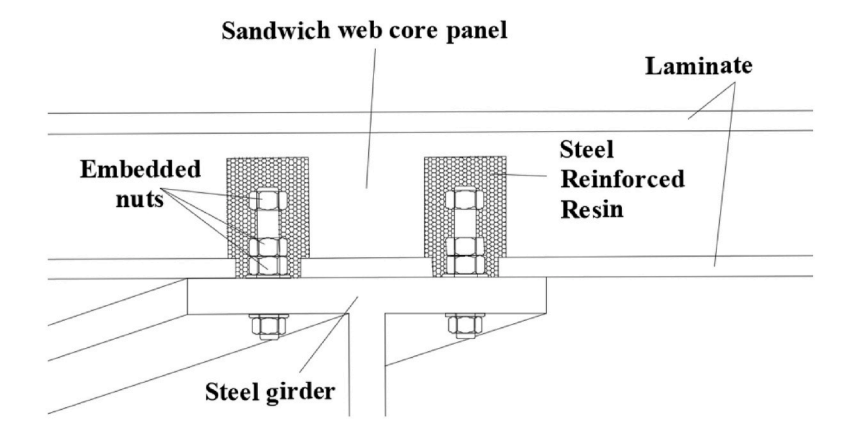


Fig. 2. Steel reinforced resin (SRR) material forming a connector for FRP bridge decks.



(a) Demountable shear connector for steel-concrete composite floor systems [1]



(b) Shear connector between composite deck panel and steel girder [2]

Fig. 1. Cross section of connections with SRR material as injection filler in different applications.

provided by structural metal components. Therefore, in the context of FRP-to-steel applications, the injected SRR is in a semi-confined state [13,14].

The compressive stresses generated within the SRR material when applied in connectors play a critical role in the joint's fatigue performance. Therefore, this study aims to investigate the compressive response of SRR under monotonic, incremental cyclic, and high-cycle fatigue loading without confinement. A custom triaxial test setup is employed for monotonic loading to apply active confining pressure, enabling a more accurate assessment of pressure-dependent behaviour. Additionally, incremental loading tests under unconfined conditions explore the relationship between plasticity, stiffness degradation, and damage accumulation. To complement the experiments, micromechanical finite element models simulate the interaction between resin and steel particles, incorporating interface damage and frictional contact. These models provide further insight into stiffness evolution, failure mechanisms, and the varied behaviour observed in tension versus compression, including differential Poisson's ratios.

2. Description of experimental work

2.1. Details of specimens

Cylindrical specimens, each with an average diameter of 26.0 mm and a length of 52.0 mm, are prepared by integrating steel particles of nominal size class S330, conforming to standard J444, into an unsaturated polyester polyurethane, UPE + PU, resin (AQR 1025/B25), which was selected based on previous work [15]. The ratio of steel particles to resin is maintained at 4:5. No compaction is applied during specimen fabrication, as it is deemed unnecessary. This is due to the use of open cylindrical moulds and a manufacturing process similar to the method used for producing the injected SRR connectors. In this process, steel particles are first placed into the mould, and resin is injected from the bottom upwards using a pressure gun. This approach ensures uniform resin distribution around the steel particles. Once the steel particles fill the mould to the required specimen length, the excess hardened resin layer that forms at the top is removed using laser cutting. This step ensures a flat and even surface, essential for conducting the compressive tests correctly.

The experimental test matrix is presented in Table 1, summarizing the number of tests for each loading condition and the corresponding confinement level applied in this study. All tests are done under room temperature and moisture conditions. Three monotonic tests without confinement are conducted to determine the compressive strength. Following these destructive monotonic tests, three incremental cyclic loading tests are performed to generate the material's hysteresis loops. Finally, cyclic loading is applied at three different stress levels, with three specimens tested at each level.

2.2. Test setup and instrumentation

The application of compressive force varies depending on the confinement conditions, necessitating the use of different machines (see Table 1 last column) and methods. For static tests conducted without

Table 1Overview of experiments for SRR material characterization under compression.

Loading	Minimum load	Confinement level	Coupons	Machine
Monotonic	NA	Unconfined	3	MTS-50
	NA	10 MPa	1	MTS-25
	NA	20 MPa	1	MTS-25
	NA	30 MPa	1	MTS-25
Incremental cyclic	NA	Unconfined	3	UTM-5
Cyclic (fatigue)	-20 kN	Unconfined	3	MTS-50
	-24 kN	Unconfined	3	MTS-50
	-30 kN	Unconfined	3	MTS-50

confinement, the compressive strength of the specimens is evaluated using an MTS actuator with a capacity of 250 kN. The system is equipped with three Linear Variable Differential Transformers (LVDTs) to accurately measure the average contraction of the specimens between the plates where load is applied. The experimental setup, including the placement of the sensors, is illustrated in Fig. 3. All tests are performed under a LVDT-controlled regime at a speed of 0.01 mm/s. This setup is also employed for incremental cyclic loading tests, where the loading and unloading rates are consistent with those used in the monotonic tests. The cycles of loading, unloading, and reloading are depicted in Fig. 4.

This same setup, Fig. 3b, is further utilized for cyclic loading tests, where the load is applied in a sinusoidal form. Force control is regulated by a peak controller to maintain a constant peak force, even as the material properties degrade. These tests are conducted at a frequency of 4 Hz, under room temperature and dry environmental conditions. A stress ratio of R=10 is used for all specimens, meaning they are subjected to compressive loading only, with no load relief during testing.

The triaxial compression tests are conducted using a servo-controlled loading machine with a maximum capacity of 500 kN and accuracy of 0.001 kN. The experiments take place at room temperature on intact samples, utilizing a Hoek cell embedded in the 500 kN machine to apply confining pressure using oil under load control without pore pressure. The testing system, as shown in Fig. 3c, uses an external ISCO 65D syringe pump to control the confining pressure with an accuracy of 0.5 %. Both the axial force and confining pressure are applied simultaneously, with a constant displacement ratio of 0.6, until reaching the desired confinement level of 10, 20, or 30 MPa. Once reached, the pressure is maintained constant, and only the compressive load is applied under strain control at an axial strain rate of 0.0005 s $^{-1}$.

During the tests, axial displacement, axial force, and confining pressure are logged at 1-s intervals, with vertical deformation measured using two LVDTs with an accuracy of 1 μm . The tests continue until a displacement limit of 1.95 mm is reached, before the point the system reaches its deformation capacity, which is 2 mm. Each confinement level is tested with one monotonic test, as preliminary trials showed minimal variation at lower confinement pressures.

3. Compressive behaviour of SRR material under monotonic loading

3.1. Uniaxial compressive behaviour under static loading

The compressive strength of the cylindrical specimens is determined by dividing the applied force from the actuator by the initial cross-sectional area of the specimen, calculated as $A=\pi \cdot r^2$, where r=13.0, resulting in an area of $531~\mathrm{mm}^2$. Strain is calculated as the ratio of the specimen's contraction to its initial height. The Young's Modulus of the SRR material in compression is obtained from the slope of the initial linear portion of the stress-strain curve. For accuracy, it is consistently measured within the stress range of 40 MPa–60 MPa, which lies below the onset of nonlinearity. This method ensures that the measurement is unaffected by any potential initial settling of the specimen during testing.

The stress-strain curves for the unconfined SRR specimens subjected to both monotonic and incremental cyclic loading are presented in Fig. 5. The maximum compressive strength recorded under monotonic loading was approximately 84.3 MPa, which decreased by only 2.85 % under incremental loading. Under both loading conditions, neither the Young's modulus nor the stress at the onset of non-linearity and the ultimate compression strength vary significantly. A collection of the experimental results is given in Table 2.

The stress-strain curve for the monotonic loading test is fairly linear until 80 MPa of compressive stress. Then it shows a distinct peak followed by a gradual decrease in stress, indicating strain softening behaviour after the material reaches its maximum compressive strength.



(a) SRR coupon



(b) Unconfined test setup



(c) Triaxial test setup

Fig. 3. Specimen geometry and experimental setups for characterizing the compressive behaviour of SRR material.

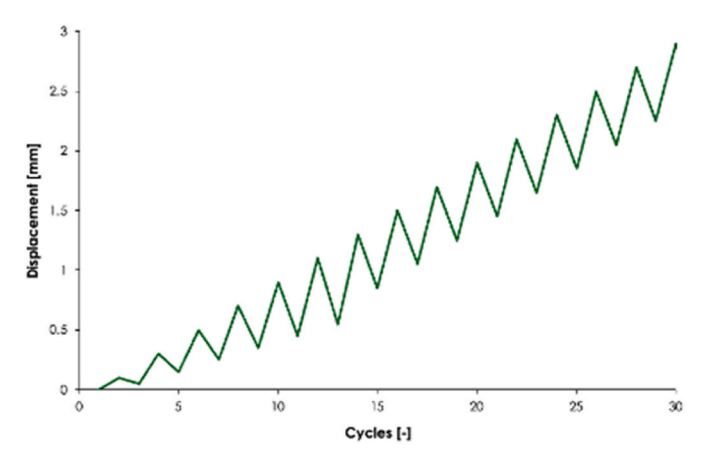
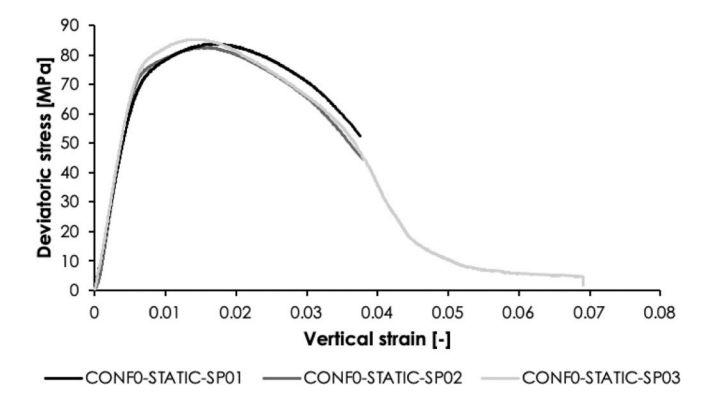
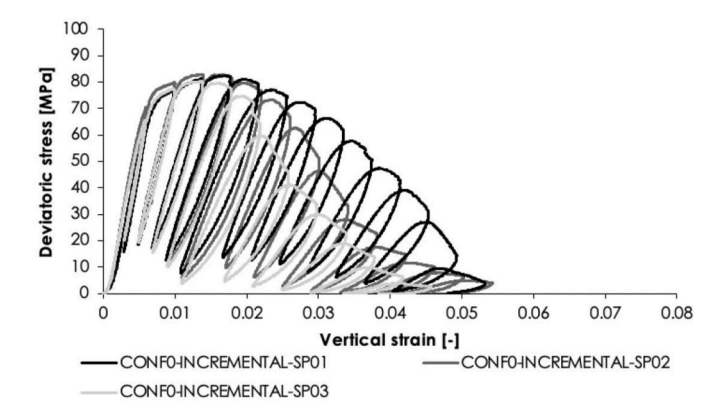


Fig. 4. Incremental cyclic loading protocol.



(a) Monotonic loading



(b) Incremental loading

Fig. 5. Stress strain curves under uniaxial compression of SRR material.

This post-peak reduction suggests that the SRR material begins to lose its load-bearing capacity due to micro-cracking and localized damage. Similarly, during the incremental cyclic loading tests, an increase in residual strain is observed after each unloading cycle, further reinforcing the presence of strain softening. The progressive accumulation of residual strain and the change in the slope of the reloading loops in incremental cyclic tests highlight the dual nature of nonlinear behaviour, attributed to both damage, resulting in a decrease in material stiffness, and plasticity, leading to permanent deformation.

To quantify material degradation, a scalar damage variable D was

Table 2Experimental results of compression tests under monotonic loading in unconfined condition.

Loading	Specimen	Young's modulus (GPa)	Compression strength (MPa)
Monotonic	1	13.2	84.3
	2	13.0	83.9
	3	13.1	84.9
	Mean	13.0	84.3
Incremental	1	11.8	82.5
cyclic	2	11.4	82.9
	3	13.1	80.2
	Mean	12.1	81.9

defined as:

$$D = 1 - \frac{E_i}{E_0} \tag{1}$$

where E_i is the secant stiffness at the i^{th} loading cycle and E_0 is the initial elastic modulus from the first cycle. This definition reflects the reduction in load-carrying capacity as the material accumulates microstructural damage over repeated cycles.

The results from the incremental cyclic tests further highlight the progressive nature of damage and plastic deformation in the SRR material. As evident in Fig. 6, plastic strain remains negligible during the initial loading cycles, while the total strain accumulates. This suggests that damage is the dominant mechanism driving stiffness degradation at the early stages, as it correlates with the relatively linear increase in damage observed in Fig. 7. The gradual onset of plasticity is evident later in the test, as $\epsilon_{\rm pl}$ begins to grow more significantly, aligning with the progressive accumulation of permanent deformation.

Additionally, the hysteresis loops of the SRR material based on the incremental cyclic tests provide insights into energy dissipation due to material damage and micro-cracking. The area within the loops evolves with the number of cycles, reflecting the viscous behaviour of the material. It should be noted that the incremental cyclic loading is applied at a relatively low rate (approximately 1.5 min/cycle), which may have introduced creep effects. This time-dependent deformation could contribute to the overall strain accumulation, potentially affecting the ratio between damage and plasticity contributing to the non-linear behaviour of the material. To better distinguish between damage caused by cyclic loading and creep, further analysis, such as tracking the evolution of residual strain or conducting dedicated creep tests, would be necessary. The damage versus plastic strain curves, constructed from these loops, provide an initial indication of how the material deforms plastically and accumulates damage over time, though a more comprehensive approach is required to fully isolate the impact of creep.

The relationship between damage, D, and plastic strain, $\epsilon_{\text{pl}},$ for the

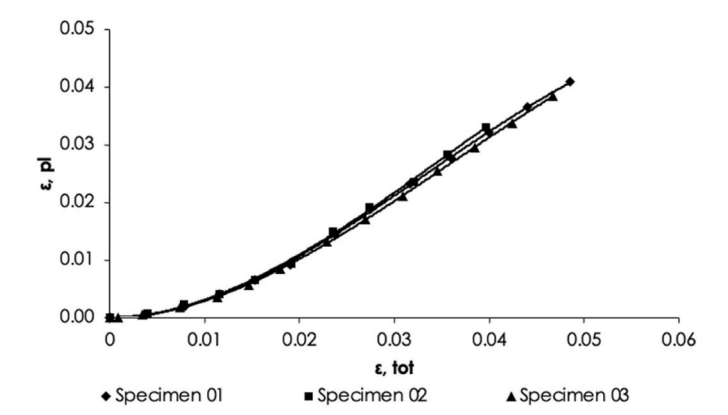


Fig. 6. Plastic strain versus total strain of SRR material under compression in unconfined conditions.

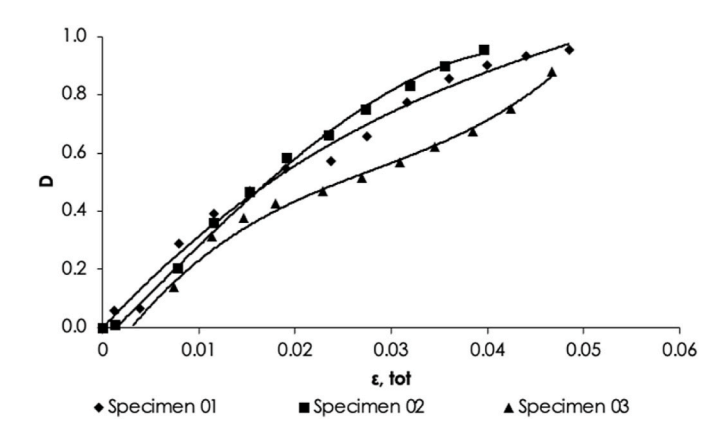


Fig. 7. Damage progression versus total strain of SRR material under compression and in unconfined conditions.

three specimens, as shown in Fig. 8, exhibits a three-stage progression. In the initial stage $(\epsilon_{pl} < 0.015)$, damage accumulates gradually, indicating that microstructural degradation occurs before significant plastic deformation develops. The intermediate stage is characterized by a steady increase in plastic strain and accelerated damage growth, suggesting that plasticity increasingly contributes to the material's degradation. In the final stage $(\epsilon_{pl} > 0.03)$, damage rises sharply and approaches saturation, reflecting extensive microcracking and stiffness loss

Despite some variations in the rate of damage progression between the specimens, all curves follow a third-degree polynomial trend, emphasizing a typical 3-stage development form of interaction between plastic deformation and material degradation. The results suggest that softening is primarily driven by plastic strain in the second (steady) stage, with damage dominating in the primary and tertiary stage of softening. This consistency across the specimens tested under incremental (low-cycle) loading indicates that the SRR material may exhibit predictable fatigue behaviour under high-cycle compressive loading.

The post-peak behaviour of the monotonic and incremental cyclic loading tests varies among the tested specimens, which is to be expected. Specifically, the post-peak behaviour exhibits noticeable variation due to the inherent heterogeneity of the SRR material, where the interaction between steel particles and resin leads to localized stress concentrations and varying failure mechanisms on a microscopic scale. Additionally, particle sliding, rearrangement, and dilatancy effects contribute to the observed differences, as the material undergoes micro-cracking and damage localization after reaching peak load. Regardless of the loading type applied, a consistent failure mode was observed across all specimens by the end of the test. As shown in Fig. 9, the predominant failure involved mainly diagonal and some longitudinal cracks, culminating in the final fracture of the specimen through "explosive" spalling of some

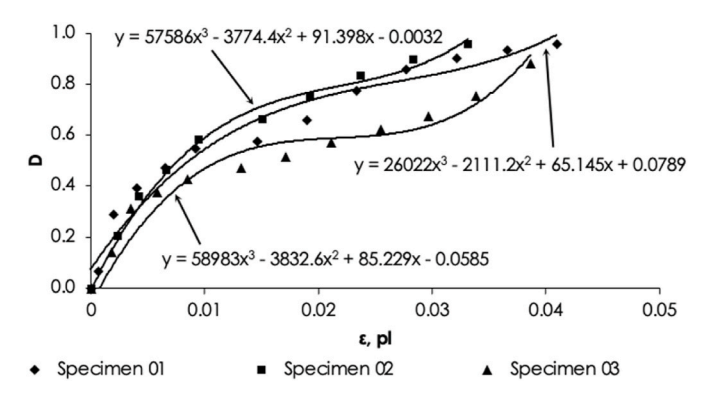


Fig. 8. Damage progression versus plastic strain of SRR material under compression in unconfined conditions.

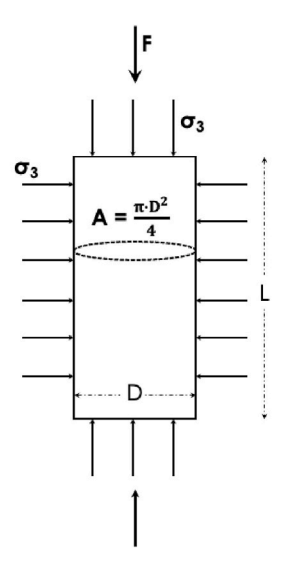


Fig. 9. Failure mode of SRR material under monotonic uniaxial compression.

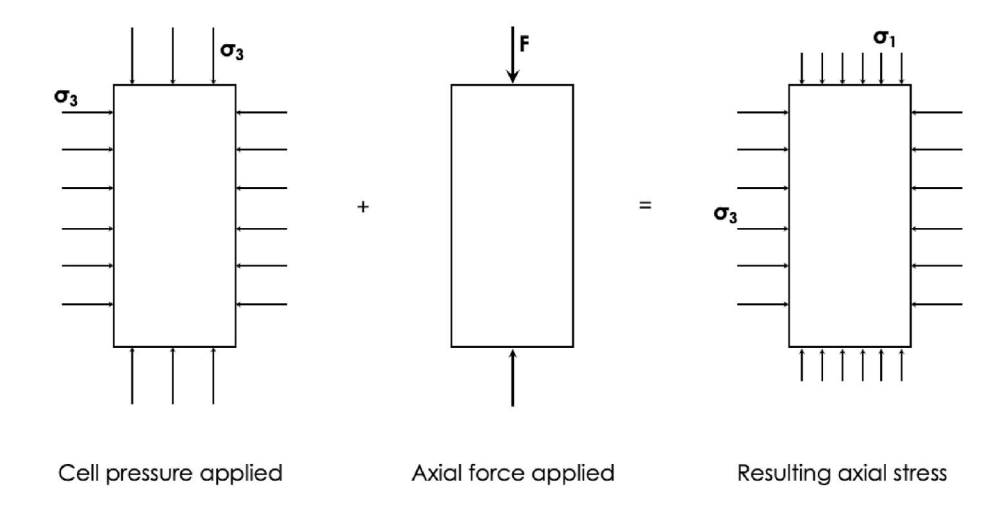
specimens.

3.2. Triaxial compressive behaviour under static loading

Three triaxial tests are performed, with the confining pressure varying from 10 MPa to 30 MPa. During each test, an increasing longitudinal compressive load is applied alongside the confining pressure until the desired confining pressure, σ_{3} , is reached. Once this target confining lateral pressure is achieved, it is held constant, and only the axial load, F, is progressively increased during what is considered the shearing (deviatoric) phase of the test. The additional stress from the load is applied solely in the axial direction and is calculated by dividing the axial force by the initial cross-sectional area (A) of the cylindrical specimen. The total axial stress experienced by the SRR material is equivalent to the major principal stress (σ_1) and can be expressed as:



(a) Cylindrical specimen under triaxial compression



(b) Loading stages of triaxial test

Fig. 10. Principles of triaxial compression test.

$$\sigma_1 = \sigma_3 + \frac{F}{A}$$

The deviatoric stress component (q) for the confined SRR specimens is determined by subtracting the applied confining pressure (minor principal stress, σ_3) from the vertical stress (major principal stress, σ_1). The deviatoric stress component is progressively increased until either the specimen experiences failure, typically through cracking or spalling, or until a plateau is reached, indicating that the material has undergone plastic deformation or strain softening. Fig. 10 illustrates the principles of the triaxial compression tests.

The deviatoric stress component versus axial strain curves are presented in Fig. 11. A clear trend of increasing deviatoric stress with higher applied confining pressure is observed, aligning with conclusions drawn from the literature. All three specimens exhibit only slight variation in initial stiffness. The stiffness for 10, 20 and 30 MPa of confinement pressure is 10.5, 11.3 and 12.1 GPa, respectively, showing a slight increase with rising pressure. However, given the minor variations between the different confinement levels, this change is more likely attributed to statistical variability rather than a significant shift in material behaviour.

The most significant change occurs at the onset of nonlinearity, which directly impacts the maximum deviatoric stress that the SRR material experiences and confirms that the SRR material benefits from confinement, as it enhances its load-bearing capacity. The transition from the elastic to nonlinear region is smooth, indicating that the SRR material gradually absorbs energy and deforms plastically and is not exhibiting a sharp yield point. This gradual transition highlights the ductile nature of the material under confinement.

Notably, none of the specimens exhibit failure; instead, they reach a plateau in deviatoric stress, which is maintained until the test is manually stopped. This plateau behaviour suggests that the SRR material under confinement can sustain a high level of stress without immediate failure, potentially indicating stable plastic flow or strain hardening. This behaviour has important implications for the material's application in structures, where maintaining stress without failure could enhance safety and durability.

Even though failure is not reached in any of the tests, the plateau phase suggests that micro-cracking or particle rearrangement is occurring at the micro-structural level, delaying complete failure. A representative specimen after triaxial compression is shown in Fig. 12, confirming the absence of visible macroscopic failure or cracking. To better understand the nonlinear behaviour and the plateau observed in the experimental tests, micro-mechanics modelling, conducted in Section 5, is used to investigate the underlying mechanisms. The modelling provides insights into how the interaction between the steel particles and the resin matrix contributes to the material's overall response, particularly the transition to nonlinearity and the stable plateau phase.

Comparing the triaxial test results with the unconfined monotonic

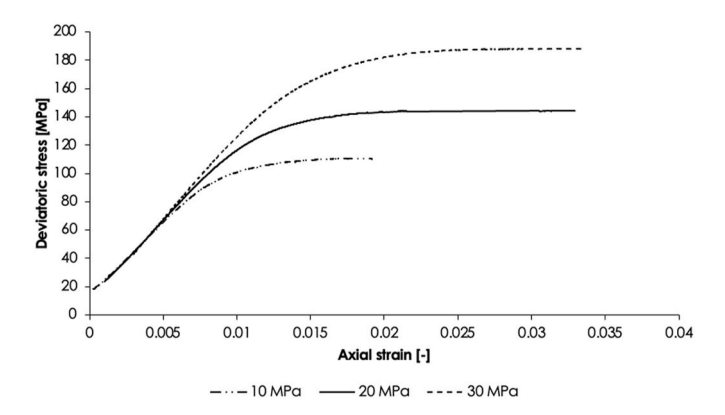


Fig. 11. Deviatoric stress versus axial strain curves for SRR material during the shearing phase of triaxial compression tests at varying confining pressures.



Fig. 12. SRR specimen after triaxial compression test at 20 MPa confining pressure.

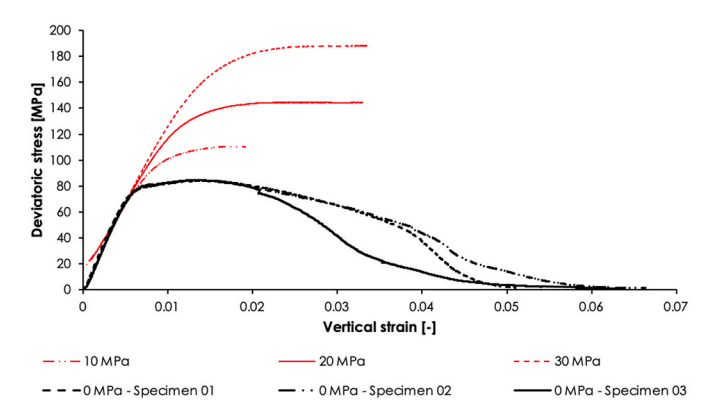


Fig. 13. Deviatoric stress versus axial strain curves for SRR material under unconfined and confined conditions at various confining pressures.

tests on the SRR material highlights the significant improvement in load-bearing resistance under confinement, as shown in Fig. 13. It is also clear that confining pressure generally enhances the ductility of the SRR material. This behaviour is typical for granular composites, suggesting that confinement plays a crucial role in restricting lateral expansion and delaying the onset of failure, thereby improving both the material's strength and ductility. The increased confining pressure allows the SRR to sustain higher deviatoric stresses without experiencing announced failure, making it particularly suited for applications where lateral confinement or triaxial stress states are present. Such a scenario is expected in the application of SRR as an injection material for connectors in composite decks. In these cases, the SRR material is surrounded by the composite material of the deck facing, which can provide mild confinement conditions.

An important point of attention is the difference in the slope of the deviatoric stress versus axial strain curve, which reflects the Young's modulus. The stiffness of the unconfined SRR material appears to be higher than that observed under the three confinement levels. This discrepancy is attributed to the use of different testing apparatus for the two sets of tests, with different machines and LVDTs potentially leading to measurement variations. Despite this experimental outcome, it is hypothesized that the SRR material being evaluated in this study, with its 80 % steel particle volume fraction, should exhibit a similar Young's

modulus under both unconfined and confined conditions. This is because the material's elastic behaviour is primarily governed by the densely packed steel particles, which dominate the load-bearing mechanism in both scenarios. Further insights into this hypothesis will be explored through micro-mechanics modelling in Section 5, which aims to shed light on the underlying mechanisms contributing to the stiffness in these tests.

4. Compressive behaviour of SRR material under cyclic loading

4.1. Testing procedure

In this section, the fatigue behaviour of the SRR material under uniaxial compression is examined. These tests are conducted without confinement, as the applied stresses are maintained within controlled levels to evaluate the material's response. The focus on unconfined conditions aims to capture the high-cycle fatigue behaviour of the SRR material and to predict its performance in applications with mild confinement, such as when applied in composite/hybrid bridge decks.

As previously mentioned, the unconfined test setup is used for this series of cyclic experiments, with three minimum force levels of -20, -24, and -30 kN applied to cylindrical SRR specimens. The stiffness values of the specimens are computed for each cycle by dividing the force range by the corresponding LVDT displacement range.

4.2. Stiffness degradation curves and failure mode

Fig. 14 presents the normalized stiffness values for all specimens over their fatigue life. The pattern is consistent across most specimens: stiffness gradually decreases in a roughly linear manner until approximately 40 % of the specimen's life, at which point the degradation rate accelerates exponentially until failure.

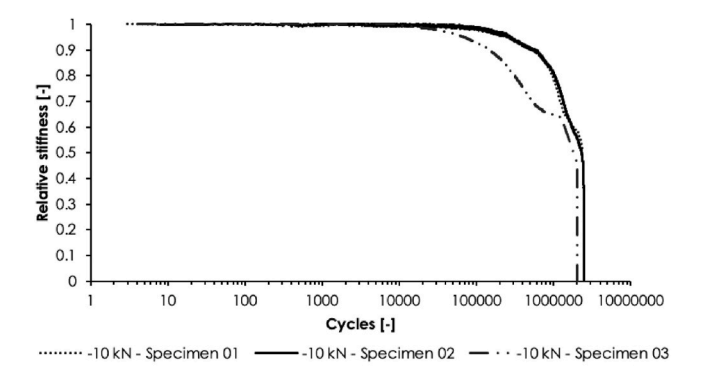
In the monotonic loading tests, the main failure mode of the SRR material is a diagonal crack, which is a typical failure mode under such conditions due to the high stress concentration along the shear plane. In contrast, during the cyclic loading tests, the failure mode was more complex, resembling a clepsydra (hourglass) pattern, where the specimen fractured into several pieces.

The clepsydra-shaped failure observed in the cyclic loading tests is a result of cyclic fatigue damage, leading to multiple crack initiations at stress concentration zones near the top and bottom of the specimen. These cracks propagate in a triangular pattern, eventually constricting the midsection and causing the specimen to break into several pieces, forming the characteristic hourglass shape, as depicted in Fig. 15. The failure mechanism is driven by the progressive weakening of the material under cyclic stress, resulting in distributed damage rather than a single failure plane.

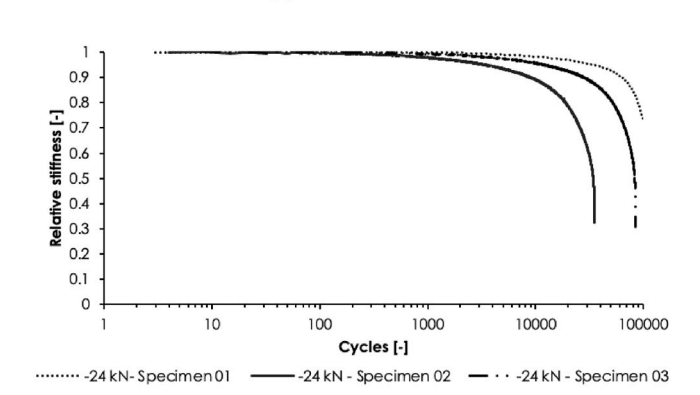
4.3. σ-N curve of SRR material under unconfined compressive loading

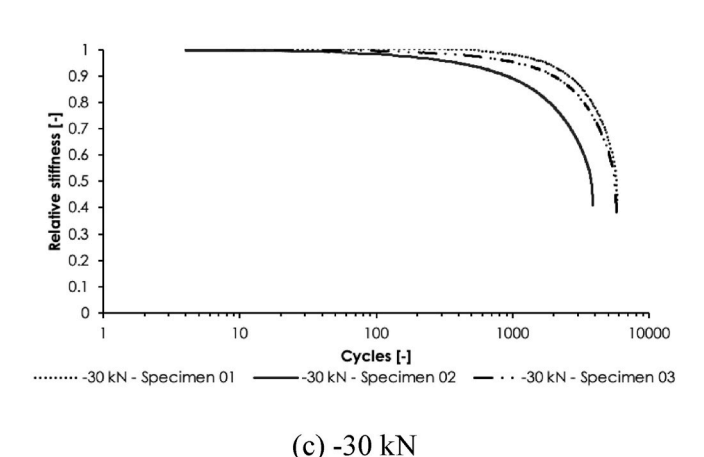
Interestingly, during fatigue tests conducted under indirect tensile loading on the same SRR material presented in earlier work [16], the slope of the $\sigma\textsc{-N}$ curve was calculated to be 14.27, which is very close to the value of 14.63 obtained in the compressive fatigue tests, and presented in Fig. 16. The similarity in the slope across different testing methods indicates a consistent relationship between stress and fatigue life for the SRR material, regardless of the loading mode.

This close agreement suggests that the material exhibits similar fatigue sensitivity in both tensile and compressive fatigue scenarios. Specifically, in both cases, even slight increases in stress lead to a significant reduction in fatigue life. This consistency highlights the material's inherent fatigue behaviour, which can be useful when designing components subjected to various loading conditions, as the fatigue life predictions across different loading modes are comparable. In addition, such a steep slope of the fatigue behaviour indicates that a cut-off limit for connectors may exist. In other words, with a proper design of the



(a) -20 kN





(b) -24 kN

Fig. 14. Normalized stiffness values for SRR material under uniaxial compression over their fatigue life.

connection (e.g. appropriate connector diameter), the load level can be replicated to a sufficiently low stress level that in turn will result in an infinite life of the connector.

5. Numerical investigation: micromechanical modelling of SRR material

Heterogeneous materials like SRR, composed of steel particles embedded in a resin matrix, exhibit distinct properties and interact at a microscopic scale. Micro-mechanical modelling typically involves numerical simulation of a representative volume element (RVE), which captures these complex interactions and reflects the material's local heterogeneity. This method reveals specific micro-structural details

Fig. 15. Failure mode of SRR material under cyclic uniaxial compression (fatigue).

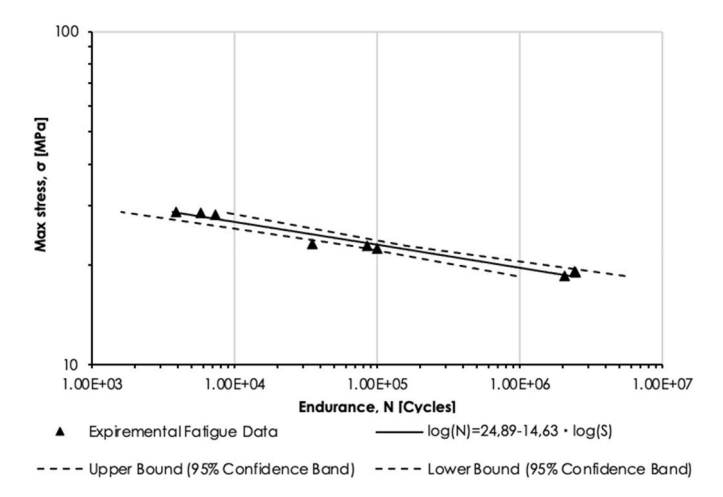


Fig. 16. Preliminary $\sigma\textsc{-N}$ curves (R = 10) for SRR loaded in compression at 25 $C^{\circ}.$

responsible for non-linear material behaviour, providing valuable insights into SRR stiffness, interfacial strength, and failure mechanisms. Similar micromechanical approaches have been applied in thermal studies of highly filled composites, where particle contact and interface properties were shown to significantly influence material behaviour [17].

This section focuses on validating the behaviour of a fine-scale FE model with a limited amount of steel particles and resin interacting in a microscopically small structure against the unconfined and confined compressive experimental static behaviour of the SRR material, as discussed in the previous section. The use of a periodic hexagonal packing follows common micromechanical modelling strategies for particulate composites, where idealized arrangements enable efficient analysis of stress distribution and interfacial effects. Prior studies have shown that hexagonal packing can accurately reproduce the macroscopic stiffness and local stress behaviour of composites with circular inclusions [18]. Bayat and Aghdam [19] demonstrated that hexagonal RVEs more accurately capture local stress distributions and yield behaviour in fibrous composites compared to square arrangements, further validating this choice. While the current model uses this idealized structure, real SRR material likely exhibits non-uniform packing. As demonstrated in Refs. [20,21] such particle clustering can significantly reduce failure strain, increase local stress concentrations and promote early interface damage. This suggests that although the present model is representative of average conditions, future work could incorporate spatial randomness to assess the influence of clustering on damage evolution more comprehensively.

5.1. Description of micromechanics model

A three-dimensional periodic hexagonal arrangement of steel particles within the resin bath is modelled, representing a cubic RVE with dimensions 3 x 3 \times 3 mm, as shown in Fig. 17. The steel particles, each 1

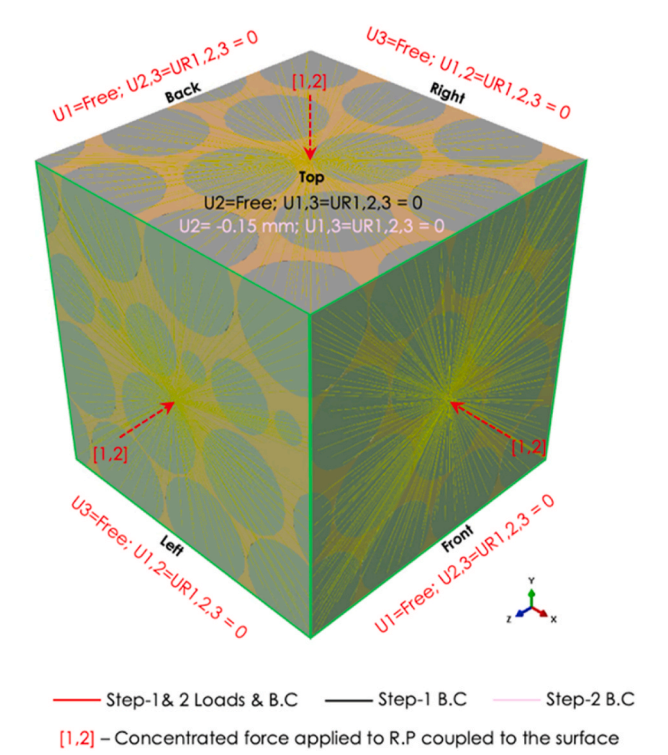


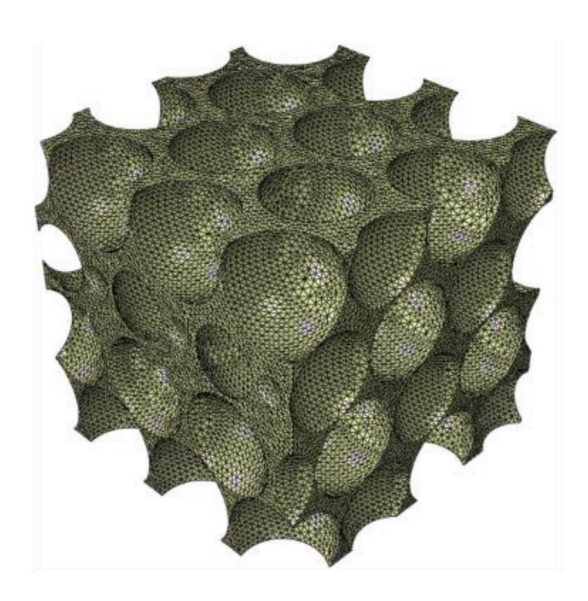
Fig. 17. FE model of the zoomed-in SRR material system.

mm in diameter, are distributed spatially with a global particle volume fraction of 75 %, consistent with compaction levels reported by Refs. [3, 16]. The mesh model is created using geometrically versatile linear tetrahedron elements with four nodes (C3D4) for both steel particles and resin with a global mesh size of 0.05 mm, as indicated in Fig. 18. This mesh size is considered satisfactory based on a mesh sensitivity study and enables accurate representation of the microstructural interactions and response of SRR under static loading conditions.

The modelled components are assigned two distinct material properties. The steel particles have isotropic elasto-plastic properties (E = 210 GPa; $\nu = 0.3$), with the nominal stress-strain relationship for plasticity assuming 355 MPa as the onset of yielding followed by linear hardening towards 480 MPa with 20 % plastic strain [22]. The resin is modelled using an elasto-plastic (E = 3 GPa: $\nu = 0.35$; $\rho = 2 \, kg/m^3$) constitutive law with isotropic hardening. Although polymeric resins can exhibit rate-dependent and viscoelastic effects, a rate-independent model was adopted here due to the quasi-static loading conditions. Instead of a simplified bilinear idealization, the resin's plastic response is defined using multiple yield points to capture a more gradual hardening behaviour. A conservative yield stress of 70 MPa was selected based on experimental data, accounting for imperfections such as local voids, surface roughness, and residual stresses not explicitly captured in the micromechanical geometry. The plastic response is defined according to Table 3.



(a) Steel particles



(b) Resin matrix

Fig. 18. Mesh applied in both parts that form the SRR material.

To capture the post-peak response, the plasticity model is coupled with a ductile damage material model, where damage initiation and evolution depend on the stress triaxiality. While the same material parameters are used for both tensile and compressive simulations, the ductile damage model results in different behaviour under varying loading conditions due to the triaxiality-dependent fracture strain. In particular, a higher fracture strain was defined for negative triaxialities (compression) to delay damage initiation and better match the compressive experimental response. The complete set of input parameters used in the numerical model is presented in Table 3.

The damage initiation criterion is defined by the equivalent plastic strain at the onset of damage, $\bar{\epsilon}_0^{pl}=0.025$, dependent on stress triaxiality θ . For this quasi-static analysis, strain rate effects are neglected due to slow load application. The equivalent plastic strain at fracture, $\bar{\epsilon}_t^{pl}=$

Table 3Overview of material properties utilized in Abaqus for the resin.

Property	Yield Stress (MPa)	Plastic Strain [-]	
Plasticity	30	0	
	40	0.004	
	60	0.0135	
	70	0.025	
	60	0.04	
	50	0.05	
	Fracture Strain [-]	Stress Triaxiality [-]	
Ductile Damage Initiation	5	-0.33	
	3	0	
	0.7	0.066	
	0.5	0.132	
	0.38	0.198	
	0.26	0.264	
	0.2	0.33	

0.2, is based on findings by M.P. Nijgh [11] for $\theta=1/3$ (uniaxial tension), with an exponential dependency on triaxiality. A mode-independent damage evolution law with exponential softening is implemented. The equivalent plastic displacement at failure, $\overline{u}_f^{pl}=0.01$, is determined by multiplying the characteristic element length that equals 0.05 mm in this study, by the plastic strain accumulated during the damage process. Table 3 shows the material properties utilized in Abaqus for the resin.

To account for the interactions between component surfaces, a general contact formulation with multiple contact pairs is defined. All contact pairs between resin matrix and steel particles, as well as between the adjacent steel particles, are automatically determined and reassessed during the analysis. A finite-sliding approach using a penalty method enforces tangential contact constraints according to Coulomb friction. The friction coefficient is set at 0.2 between steel particles and 0.4 between particles and resin, with 'hard' pressure over-closure for normal behaviour.

Surface-based cohesive behaviour between steel particles and resin is modelled with a bilinear traction-separation law for interface constitutive behaviour, relating normal and shear stresses to their separations. This approach aligns with earlier micromechanical studies on particlefilled composites, where interfacial debonding and partial slip were shown to significantly influence stiffness, stress redistribution, and failure progression [23]. By default, elastic properties are based on underlying element stiffness [24]. A quadratic traction failure criterion evaluates damage initiation, assuming for simplicity equal normal and shear maximum traction of 16 MPa in this study. Mixed-mode energy-based linear softening is applied to model cohesive stiffness degradation, using the Benzeggagh-Kenane fracture criterion (exponent 2). Fracture energy parameters are determined iteratively by comparing the macro-level cylinder compressive experiments to the micro-mechanics model, and are set equal to $G_I = 0.1$ N/mm and $G_{II} = G_{III} = 0.2$ N/mm. As it can be noticed, a number of model parameters related to constituent material and interface behaviour are either assumed, simplified or phenomenologically calibrated by comparing the results to macro-level experiments. The aim here is to show the potential of such a model and use it to better understand the physical behaviour of the SRR material. Therefore, such an approximate approach in determining the parameters within the bounds of physically acceptable ranges is deemed appropriate for the aim of the study. More elaborate modelling focusing on the potential of such a micro-mechanical model to optimize and completely characterize the material behaviour, e.g. for multi/axial stress states or aging, can be conducted in the future.

The analysis of the micro-mechanical SRR model under confinement is performed in two sequential steps, as shown in Fig. 17. In Step 1, confinement is applied compressively to reference points on the cube's side faces, kinematically coupled to the corresponding surfaces. In Step 2, confinement remains constant, and a compressive displacement of

 $0.15~\mathrm{mm}$ is applied to the top and bottom faces. Abaqus/Explicit solver is utilized to resolve complex non-linear material and interface behaviour, large deformations and multiple complex contact interactions (steel particles sliding on each other). Inertial effects are minimized using mass scaling with a time increment of $0.005~\mathrm{s}$ for both the confinement (can also be understood as preloading) and the load application steps of the analysis. A smooth time-dependent load amplitude function is used with an artificial time period of $100~\mathrm{and}~300~\mathrm{s}$, respectively. The FE model without confinement includes a single step where the imposed displacement is applied.

5.2. Uniaxial compressive behaviour of micro-mechanical model

Using the defined material and interface parameters in the fine-scale FE model, stiffness, Poisson's ratio, and failure progression are analyzed to correlate the compressive behaviour across varied geometries. The stress-strain diagram in Fig. 19 shows that the initial stiffness of the micro-mechanics model closely aligns with the experimental data, exhibiting a Young's modulus of 11.7 GPa. This agreement confirms that the FE model correctly reflects the initial elastic properties of the SRR material under compression, as expected from the calibrated input parameters.

Points A, B and C indicated in the stress-strain diagram in Fig. 20 show the progression of damage at the interface between the steel particles and the resin. Notably, points B and C confirm the hypothesis concerning the development of microcracks and localized interface damage in the post-peak region. While the micro-mechanics model cannot fully capture the post-peak behaviour due to convergence limitations, it provides valuable insights addressing the modelling objectives.

The micromechanical model indicates that the nonlinear response at Point A originates from the onset of interface softening between the steel particles and resin, as well as the initial development of plastic strain in the resin, as seen in Fig. 21. At this stage, no significant cracking is observed, and damage is localized at the interface.

At Point B, peak stress is reached as the plastic strain in the resin intensifies and reaches a critical level, beyond which cracking initiates and interface degradation accelerates. This combination of advanced plastic deformation and loss of interface strength marks the beginning of significant stiffness degradation.

Point C reflects the state where microcracks are fully developed, the interface is largely deteriorated, and distributed cracking in the resin contributes to the peak and subsequent post-peak drop in load. The

combined effects of interface failure, plastic strain, and microcrack propagation govern the post-peak behaviour observed in the model.

5.3. Triaxial compressive behaviour of micro-mechanical model

To thoroughly examine and understand the effects of elevated confinement, the existing FE model was analyzed under increased confinement levels of 10, 20 and 30 MPa, similar to the experiments. The stress-strain diagram of the micro-mechanical prediction, along with the corresponding experimental results under elevated confinement, are presented in Fig. 22. The predicted Young's modulus values for 10, 20 and 30 MPa of confinement correspond to 10.4, 10.88 and 12.39 GPa, respectively. These values conform closely to the experimental values presented in Section 3.

To assess the interface damage, two points are identified for each confinement level. Points A1, A2 and A3 indicate comparable levels of interface damage at the onset of non-linearity. Similarly, points B1, B2, and B3 demonstrate consistent damage levels. This suggests that higher confinement delays the initiation of non-linearity, resulting in higher ultimate stress. The transition from the elastic region to the plateau is driven by progressive interface damage. Regions A1, A2, and A3 mark the onset and gradual progression of damage (D > 0) until its full development (D = 1) near the beginning of the plateau at a certain point in the interface. The plateau region corresponds to the full progression of interface damage in regions between the particles and the resin, as depicted in Fig. 23. The presence of confinement slows the damage evolution, promoting a smooth non-linear response and plateau formation.

In addition to interface damage, the behaviour of the resin matrix also evolves significantly with increasing confinement. The presence of lateral pressure limits the resin's lateral expansion and increases the stress triaxiality, promoting a more uniform distribution of plastic strain. This results in delayed cracking initiation and a more gradual damage evolution. Under higher confinement, the resin demonstrates enhanced ductility and load transfer capacity, contributing to the stability of the post-yield plateau. The interplay between matrix plasticity and interface degradation is therefore essential to fully capture the compressive response of SRR under triaxial stress states.

5.4. Uniaxial tensile behaviour of micro-mechanical model

The results presented above demonstrate that the micro-mechanical FE model is well able to predict the uniaxial and triaxial compressive

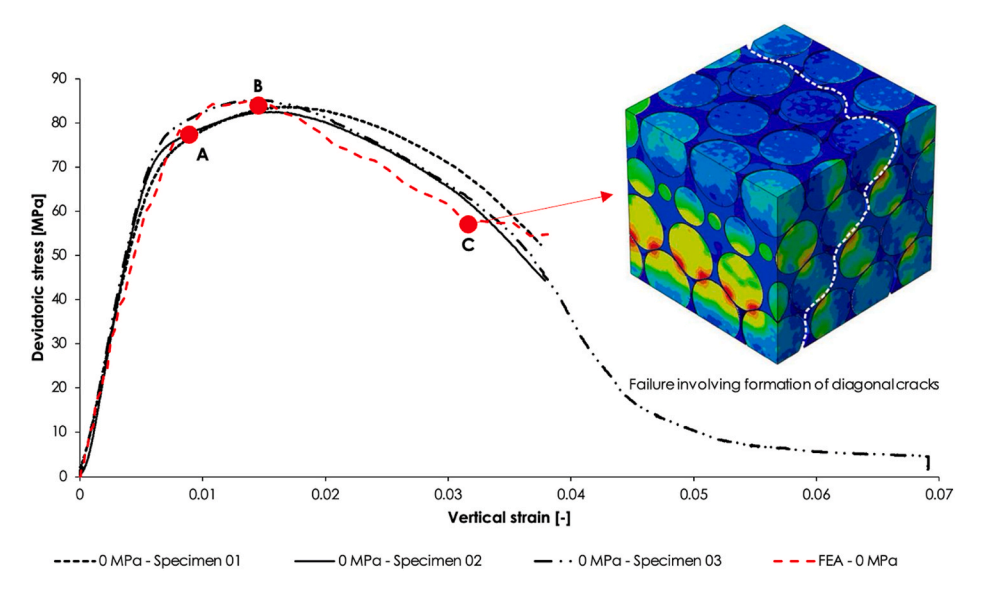


Fig. 19. Compressive behaviour of SRR as predicted by the micromechanics model.

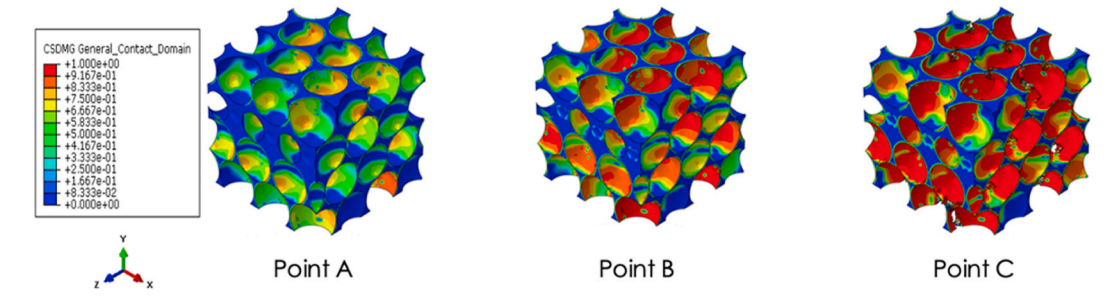


Fig. 20. Degradation of interface between steel particles and resin at various points on the stress-strain curve.

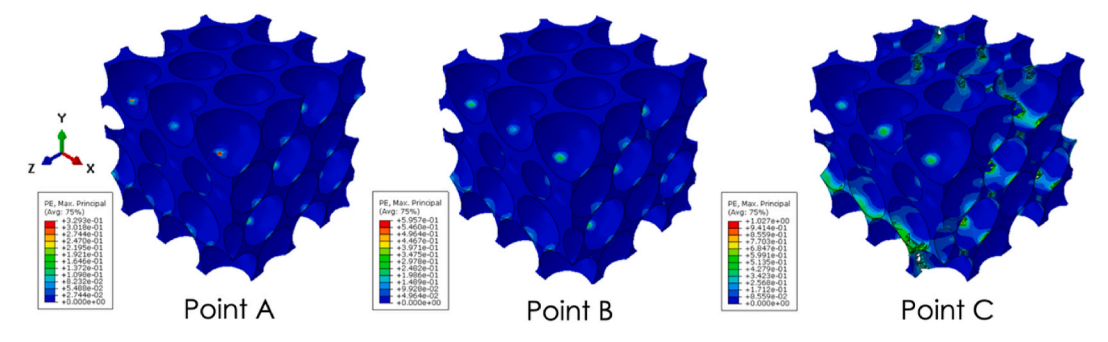


Fig. 21. Development of plastic strains in the resin at various points on the stress-strain curve.

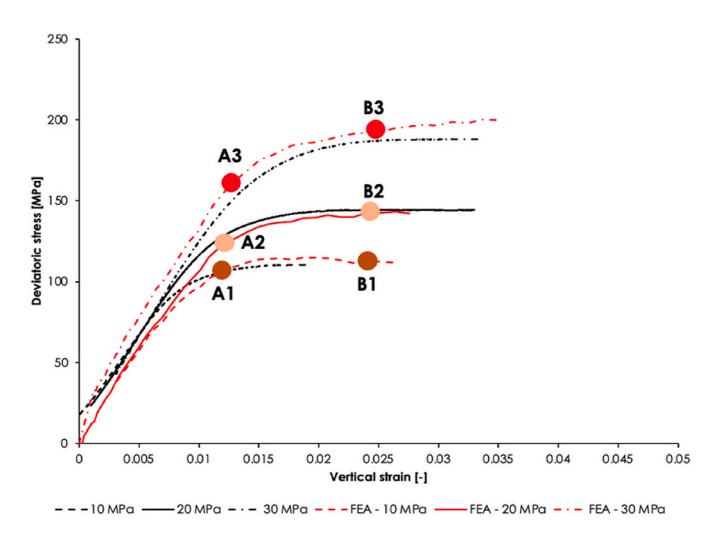


Fig. 22. Triaxial compressive behaviour of micro-mechanical FE model against the experimental results.

behaviour observed in the cylindrical steel-reinforced resin experimental campaign. With the fine-scale model validated for compressive scenarios, additional simulations are conducted without confinement to

study the tensile behaviour. The Poisson's ratio calculated from the micromechanical model under uniaxial tensile loading was found to closely match the experimental value obtained from indirect tensile splitting tests on SRR specimens with identical composition, as reported in previous work [16]. This agreement further supports the model's ability to reproduce the elastic response of the SRR material. The stress-strain response of the RVE under tensile loading is illustrated in Fig. 24.

It can be observed that the tensile strength is significantly reduced compared to the compressive strength, showing a reduction of approximately 75 %. Specifically, the tensile strength reaches 21 MPa (Fig. 24), while the compressive strength peaks at 84 MPa (Fig. 19). This reduction is primarily attributed to the lack of contact between the steel particles under tensile loading, which forces the load to be transferred almost entirely through the resin. As a result, the initial stiffness is also reduced to 5.2 GPa. This shift in the load transfer mechanism influences not only the stiffness but also the Poisson's ratio, as discussed earlier.

Fig. 25 presents the differential Poisson's ratio as a function of axial strain, based on results from the micromechanics model under both tensile and compressive loading conditions. The initial Poisson's ratio in tension is approximately 0.124, consistent with the value of 0.13 obtained from indirect tensile (Brazilian splitting) tests [16]. Under compression, the initial Poisson's ratio is significantly higher, around 0.425, reflecting the pronounced lateral expansion caused by confinement and particle interaction within the granular structure as axial

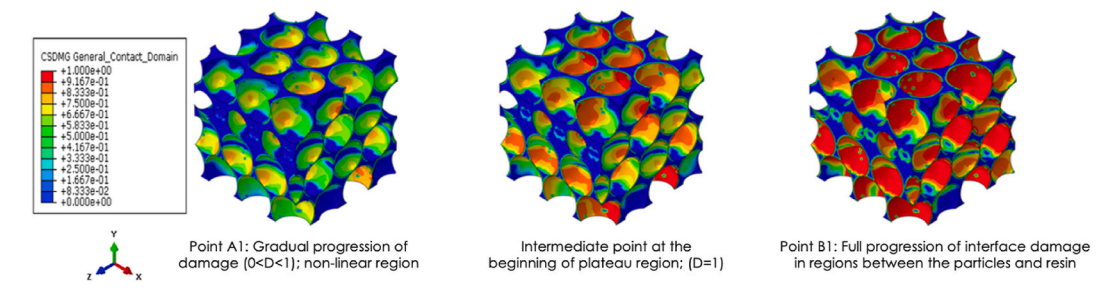


Fig. 23. Mechanisms underlying non-linearity and stable plateau behaviour.

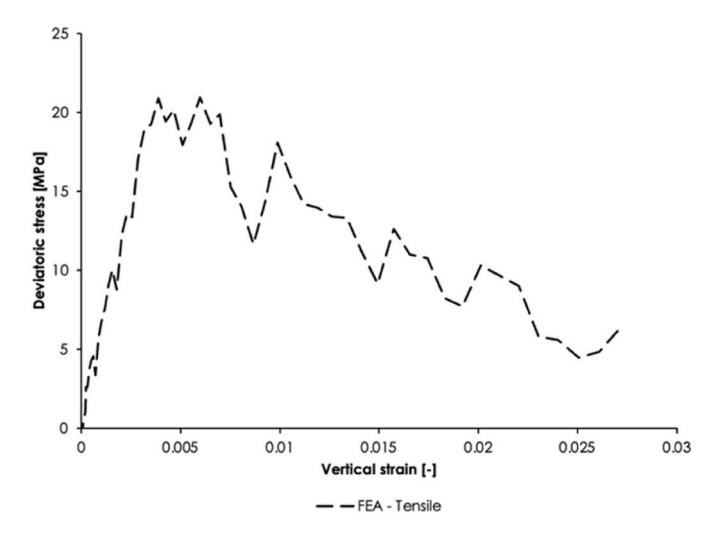
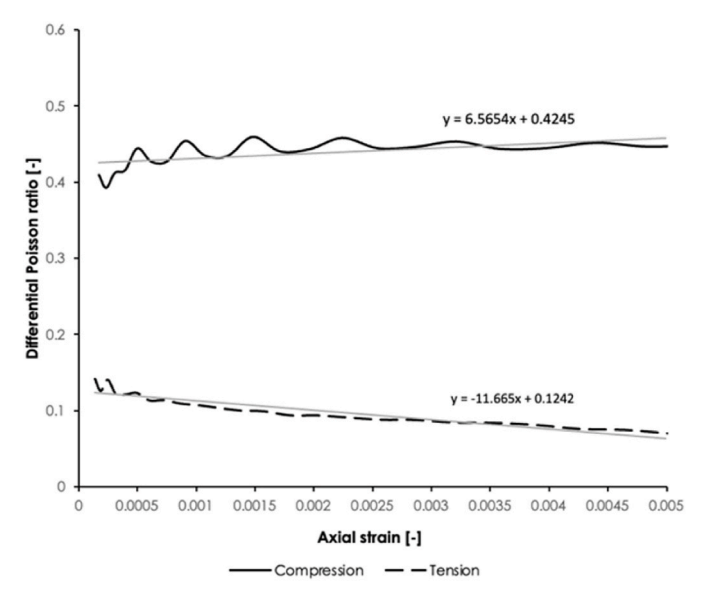


Fig. 24. Tensile behaviour of SRR as predicted by the micro-mechanical model.



 $\begin{tabular}{ll} Fig.~25.~Differential~Poisson's~ratio~response~of~micro-mechanics~model~with~no~confinement. \end{tabular}$

strain begins to develop.

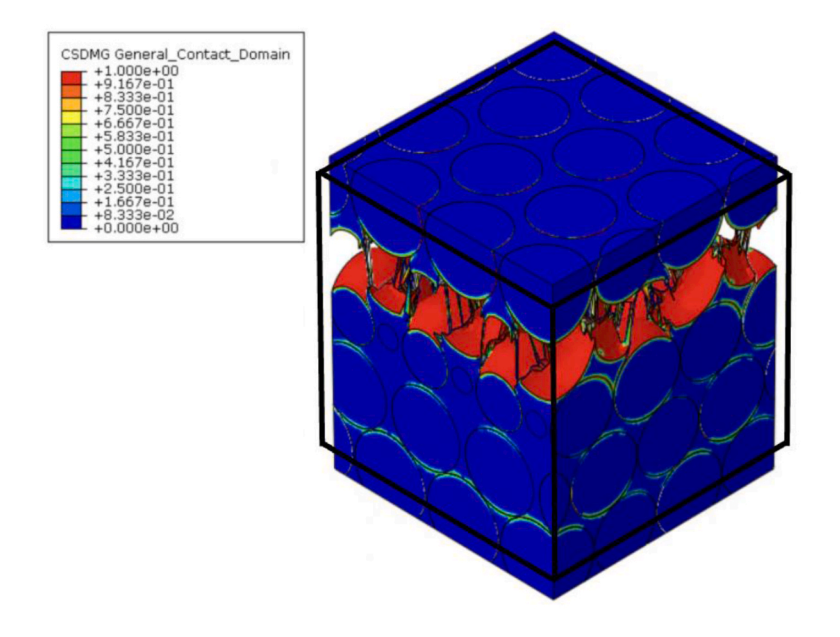
The deformed shapes in Fig. 26 provide insight into the underlying failure mechanisms. Under tensile loading (Fig. 26a), the resin matrix undergoes brittle fracture along axial planes, with limited lateral contraction. Under compression (Fig. 26b), failure is more distributed, primarily governed by progressive debonding between the resin and the steel particles, accompanied by pronounced lateral bulging. These contrasting behaviours confirm the asymmetric mechanical response of SRR and highlight that the difference arises solely from the change in load path under tension and compression. In this study, identical material properties, particle arrangement, and interface definitions were used in both simulations, meaning the observed differences result purely from how the load is transmitted through the microstructure.

6. Concluding remarks

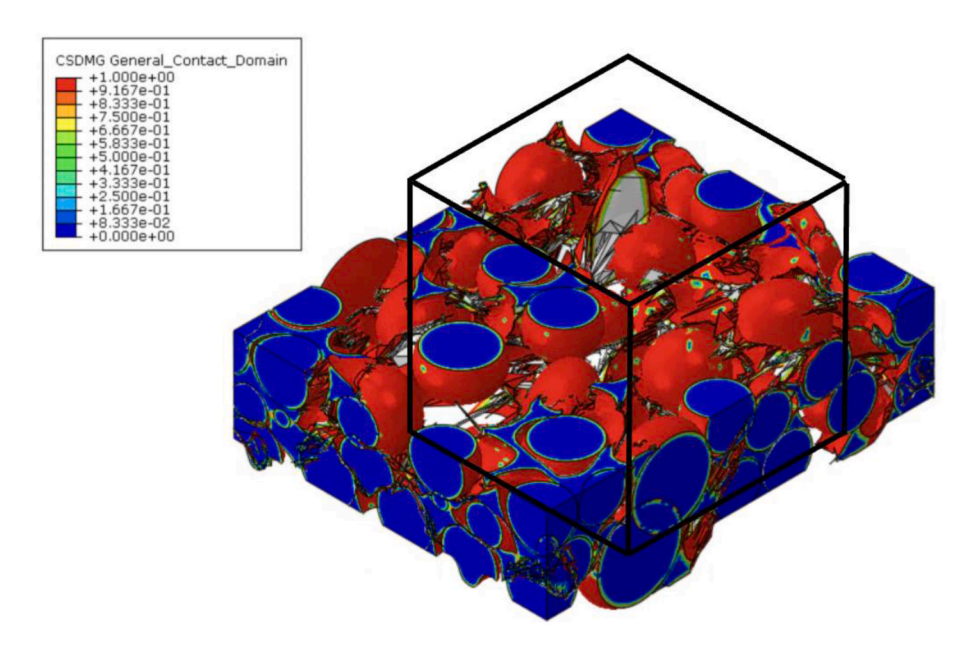
This study presented a comprehensive evaluation of the compressive behaviour of SRR material under both unconfined and confined conditions, using monotonic, incremental (low-cycle), and high-cycle fatigue tests. The experimental results provided valuable insights into the material's load-bearing capacity, stiffness, and failure modes under various stress conditions. Additionally, the impact of confinement on the SRR material's mechanical performance was assessed, highlighting its role in improving ductility and delaying failure. Despite minor stiffness variations between confined and unconfined tests, further micromechanics models were developed to better understand fundamental SRR material behaviour under confined and unconfined conditions. Based on these findings, several key conclusions can be drawn.

- 1. In the unconfined monotonic tests, the SRR material exhibited strain softening after reaching its maximum compressive strength (approximately 84.3 MPa). This was evidenced by a gradual postpeak stress reduction. Incremental cyclic load tests exhibited a stress-strain behaviour nearly identical to that observed in monotonic tests, characterized by ductile strain-softening behaviour. These tests highlighted the dual nature of the nonlinear response, attributed to the combined effects of plasticity and damage.
- 2. The triaxial tests demonstrated that confining pressure significantly enhances the load-bearing capacity of the SRR material. The material exhibited a smoother transition to peak strength under confinement, which delayed the onset of failure and improved ductility. Confinement restricts lateral expansion, delays micro-cracking, and distributes deformation more uniformly. Specifically, the confined SRR showed a maximum deviatoric stress of 190 MPa at a confining pressure of 30 MPa, compared to 84.3 MPa compressive strength in unconfined conditions.
- 3. The failure modes differed significantly between monotonic and cyclic loading. Under monotonic conditions, the SRR material consistently failed along a diagonal shear plane, splitting the specimen into two pieces. In contrast, cyclic loading induced a more complex failure mode, forming a clepsydra (hourglass) shape, with specimens fragmenting into several pieces. This clepsydra failure mode was attributed to the progressive accumulation of fatigue damage, leading to multiple crack initiations and distributed damage across several planes.
- 4. Stiffness values from the tests showed only minor differences between confined and unconfined conditions. The measured stiffness for unconfined specimens was approximately 13.1 GPa, while confined specimens had stiffness values of 10.5–12.5 GPa for confinement levels between 10 and 30 MPa. These small variations are likely due to statistical differences in testing rather than intrinsic material behaviour. It is hypothesized that SRR, with such a high steel volume fraction, should exhibit similar stiffness under both confined and unconfined conditions due to the dominance of the steel phase in governing elastic behaviour.
- 5. The fatigue data from the unconfined compressive experiments show a slope in the $\sigma\textsc{-N}$ curve, which aligns with the slope observed in the tension fatigue tests, around 14.6. This consistently steep gradient suggests that when SRR is used as a filler material in connectors for FRP–steel hybrid bridges, a fatigue cut-off limit may exist. With appropriate design, stress levels could be reduced below this threshold to achieve an infinite fatigue life. Finally, the stiffness degradation prior to failure under compressive load cycles is quantified at approximately 50 %, highlighting the progressive damage accumulation in the SRR material.
- 6. Micro-mechanics FE models reveal that the Poisson's ratio of the SRR material differs from 0.13 in tension to 0.43 in compression. Under compressive loading, a non-linear behaviour up to ultimate stress is observed which is mainly governed by damage at the resin matrix to steel pellet interface. Such a finding is confirmed in modelling also for triaxial stress states with confinement stress up to 40 % of the original compressive strength of the material.

While this study focused on testing SRR material under unconfined fatigue conditions until complete failure, future work could introduce an intermediate fatigue failure criterion to enable post-cyclic static testing



(a) Tension



(b) Compression

Fig. 26. Five-times exaggerated deformed shapes of the micromechanics model at failure under distinct loading conditions (black lines represent the undeformed cube).

on SRR cylinders. Similar approaches have been successfully applied at the connector level to evaluate residual strength and stiffness after fatigue loading [2]. Extending this methodology to material-level specimens would offer valuable insights into the damage tolerance and post-fatigue performance of the SRR material. In addition, future cyclic experiments under confined conditions could further clarify the fatigue response of SRR when used in applications where multiaxial stress states and confinement effects dominate.

CRediT authorship contribution statement

Angeliki Christoforidou: Writing – original draft, Visualization, Validation, Project administration, Methodology, Investigation, Formal analysis, Data curation. Abishek Baskar: Writing – review & editing, Investigation, Formal analysis, Data curation. Entela Kane: Writing – review & editing, Investigation, Data curation. Marko Pavlovic: Writing – review & editing, Supervision, Resources, Project administration, Methodology, Funding acquisition, Formal analysis, Conceptualization.

Declaration of competing interest

The authors declare that they have no known competing financial interests or personal relationships that could have appeared to influence the work reported in this paper.

Acknowledgements

The authors extend their gratitude to the Dutch Ministry of Infrastructure, Rijkswaterstaat (RWS), for funding this research under project number 31162138. Their generous financial support proved pivotal in the successful completion of this work.

Data availability

Data will be made available on request.

References

- [1] M.P. Nijgh, New Materials for Injected Bolted Connections a Feasibility Study for Demountable Connections, Delft University of Technology, 2017.
- [2] A. Christoforidou, M. Pavlovic, Fatigue performance of composite-steel injected connectors at room and elevated temperatures, Eng. Struct. 315 (2024) 118421.
- [3] F. Csillag, Demountable deck-to-girder Connection of FRP-Steel Hybrid Bridges, Delft Technical University, 2018.
- [4] G. Olivier, et al., Conventional vs. reinforced resin injected connectors' behaviour in static, fatigue and creep experiments on slip-resistant steel-FRP joints, Eng. Struct. (2021) 236.
- [5] F. Csillag, M. Pavlović, Push-out behaviour of demountable injected vs. blind-bolted connectors in FRP decks, Compos. Struct. (2021) 270.
- [6] G. Olivier, et al., Feasibility of bolted connectors in hybrid FRP-Steel structures, Constr. Build. Mater. 383 (2023) 131100.
- [7] H. Kupfer, H.K. Hilsdorf, H. Rusch, Behavior of concrete under biaxial stresses, in: Journal Proceedings, 1969.

- [8] J.C. Lim, T. Ozbakkaloglu, Design model for FRP-confined normal-and highstrength concrete square and rectangular columns, Mag. Concr. Res. 66 (20) (2014) 1020–1035.
- [9] J. Lankford, The effect of hydrostatic pressure and loading rate on compressive failure of fiber-reinforced ceramic-matrix composites, Compos. Sci. Technol. 51 (4) (1994) 537–543.
- [10] J. Li, C. Wang, X. Zhang, The mechanical properties and failure criteria of epoxy polymer concrete under triaxial compression, Constr. Build. Mater. 470 (2025) 140617.
- [11] M.P. Nijgh, A multi-scale Approach Towards Reusable steel-concrete Composite Floor Systems, Delft University of Technology, 2021.
- [12] B. Pedrosa, L. Bücking, M. Veljkovic, Steel-reinforced resin for bolted shear connectors: confined behaviour under quasi-static cyclic loading, Eng. Struct. (2022) 256.
- [13] F. Kavoura, et al., Mechanical properties of demountable shear connectors under different confined conditions for reusable hybrid decks, Steel and Composite Structures, An International Journal 43 (4) (2022) 419–429.
- [14] A. Christoforidou, et al., Mechanical performance of injected steel-reinforced resin connectors under different confined conditions for reusable composite structures, ce/papers 6 (1) (2023) 694–705.
- [15] Datasheet Daron 8151.
- [16] A. Christoforidou, R. Verleg, M. Pavlović, Static, Fatigue and Hygroscopic Performance of steel-reinforced Resins Under Various Temperatures, Submitted for publication, 2023.
- [17] R. Zong, et al., Numerical simulation of heat transfer of highly filled composites with spherical alumina fillers, Compos. Sci. Technol. (2025) 111064.
- [18] S. Li, General unit cells for micromechanical analyses of unidirectional composites, Compos. Appl. Sci. Manuf. 32 (6) (2001) 815–826.
- [19] M. Bayat, M. Aghdam, A micromechanics based analysis of hollow fiber composites using DQEM, Compos. B Eng. 43 (8) (2012) 2921–2929.
- [20] J. Segurado, J. Llorca, Computational micromechanics of composites: the effect of particle spatial distribution, Mech. Mater. 38 (8–10) (2006) 873–883.
- [21] Jr L. Mishnaevsky, K. Derrien, D. Baptiste, Effect of microstructure of particle reinforced composites on the damage evolution: probabilistic and numerical analysis, Compos. Sci. Technol. 64 (12) (2004) 1805–1818.
- [22] H. Xin, M. Veljkovic, Residual stress effects on fatigue crack growth rate of mild steel S355 exposed to air and seawater environments, Mater. Des. 193 (2020) 109722
- [23] E. Ghassemieh, Micro-mechanical analysis of bonding failure in a particle-filled composite, Compos. Sci. Technol. 62 (1) (2002) 67–82.
- [24] D. Systems, ABAQUS Unified FEA, 2022.